Journal of Marine Research, 61, 313–334, 2003

Interpreting wind-driven Southern Ocean variability in a stochastic framework

by Philip Sura[1,2] and Sarah T. Gille[1]

ABSTRACT

A stochastic model is derived from wind stress and bottom pressure gauge data to examine the response of the Antarctic Circumpolar Current (ACC) transport to wind stress forcing. A general method is used to estimate the drift and diffusion coefficients of a continuous stationary Markovian system. As a first approximation, the response of the ACC to wind stress forcing can be described by a multivariate Ornstein-Uhlenbeck process: Gaussian red noise wind stress drives the evolution of the ACC transport, which is damped by a linear drag term. The model indicates that about 30($\pm$10)% of ACC variability is directly driven by the wind stress. This stochastic model can serve as a null hypothesis for studies of wind driven ACC variability.

A more accurate stochastic description of the wind stress over the Southern Ocean requires a multiplicative noise component. The variability of the wind stress increases approximately linearly with increasing wind stress values. A multiplicative stochastic process generates a power-law distribution rather than a Gaussian distribution. A simple stochastic model shows that non-Gaussian forcing could have a significant impact on the velocity (or transport) probability density functions (PDFs) of the wind-driven circulation. The net oceanic damping determines whether the distribution of the oceanic flow is Gaussian (small damping) or resembles the distribution of the atmospheric forcing (large damping).

1. Introduction

Stochastic differential equations (SDEs) offer a useful formalism for describing the nonlinear dynamics of the atmosphere and ocean over a wide range of scales. The general idea of *stochastic climate models* was introduced by Hasselmann (1976) and is based on the Brownian motion analog: the observed red spectrum of oceanic fluctuations is a consequence of the amplification of low-frequency weather fluctuations. Stochastic climate models have been successful in describing ocean variability within a broad frequency band (see e.g., Imkeller and von Storch, 2001).

Despite the fact that stochastic models have been successful in providing a null hypothesis for tropical and mid-latitude oceanic variability, they have been used only

1. Scripps Institution of Oceanography, Physical Oceanography Research Division, La Jolla, California, 92093, U.S.A.

2. Present address: NOAA-CIRES, Climate Diagnostics Center, R/CDC1,325 Broadway, Boulder, Colorado, 80305-3328, U.S.A. ***email: Philip.Sura@noaa.gov***

rarely to interpret Southern Ocean variability. In one example, Weisse *et al.* (1999) studied the stochastically forced variability of the Antarctic Circumpolar Current (ACC) using a coarse resolution ocean general circulation model (OGCM). The goal of the present study is to investigate the stochastic properties of wind-driven ACC transport variability by means of an *empirical* stochastic model.

The mechanisms by which winds drive the ACC transport have been the subject of extensive debate. The debate focuses on two viewpoints: as first suggested by Munk and Palmén (1951) the wind stress over the ACC might be balanced by topographic form stress. In contrast Stommel (1957) proposed that the ACC transport might be controlled by a Sverdrup balance. Rintoul *et al.* (2001) review recent work on the subject. The variations of ACC transport in relation to winds have been studied by a number of authors (e.g., Wearn and Baker, 1980; Hughes *et al.,* 2000). More recently, Gille *et al.* (2001) used bottom pressure records from Drake Passage to show that transport fluctuations appear to be driven by the wind stress rather than wind stress curl. Our analysis will revisit the BPR observations, by fitting stochastic models to the observed time series, using methods that have been tested for other components of the climate system (see e.g., von Storch and Zwiers, 1999).

Most stochastically forced ocean models, whether simple or complex, introduce the atmospheric stochastic forcing as Gaussian white or red noise. Thus, in the models the strength of the atmospheric noise is held constant and does not depend on the state of the system. In nature, the strength of the noise may also depend on the state of the atmosphere itself, in which case the stochastic atmospheric forcing can be modeled as multiplicative noise. Sura (2003) showed that a complete stochastic description of mid-latitude sea surface wind observations requires a multiplicative (or state-dependent) white noise term. Physically, this indicates that the variability of mid-latitude winds increases with increasing wind speed. In spite of the observational evidence for multiplicative noise, the impact of multiplicative stochastic forcing on ocean models has not been explored extensively.

In this study, an empirical stochastic model is derived from wind stress and bottom pressure gauge data to examine the response of the ACC transport to wind stress forcing. Section 2 introduces the method, in which the drift and diffusion coefficients of a continuous stationary Markovian system are estimated from the observations, using a relatively new technique. The data are described in Section 3. Results presented in Section 4 are based on a first approximation, which neglects multiplicative noise and holds the stochastic atmospheric forcing constant. In Section 5 we explore the impact of more realistic multiplicative noise on the wind-driven ACC. Finally, Section 6 provides a summary and a discussion.

2. Method

In this study a general method is used to estimate the drift and diffusion coefficients of the Fokker-Planck equation for a continuous stationary Markovian stochastic process (Siegert *et al.,* 1998; Friedrich *et al.,* 2000a,b; Gradišek *et al.,* 2000). Markovian systems

can be used to represent a wide class of physical processes. We consider the dynamics of a n-dimensional system governed by the following Itô-SDE:

$$\frac{d\mathbf{x}}{dt} = \mathbf{A}(\mathbf{x}) + \mathbf{B}(\mathbf{x})\boldsymbol{\eta} \tag{1}$$

with the $n \times n$ matrix $\mathbf{B}$. $\mathbf{A}$ represents the deterministic component of the state vector $\mathbf{x}$, and $\mathbf{B}(\mathbf{x})\boldsymbol{\eta}$ is the stochastic component. Equations similar to (1) are commonly used in oceanography to represent oceanic float or drifter dispersion, where $\mathbf{x}$ represents the particle trajectory (e.g., Berloff and McWilliams, 2002). In the case of floats A_i measures the background flow field. The term $\mathbf{B}$ is constant if the variance of the float or drifter displacements is invariant in space and time.

In the discussion that follows the noise components η_i are assumed to be independent Gaussian white noise processes:

$$\langle \eta_i(t) \rangle = 0, \quad \langle \eta_i(t)\eta_i(t') \rangle = \delta(t - t'), \tag{2}$$

where $\langle \cdot \rangle$ denotes the averaging operator. This is consistent with the formalism of the Itô stochastic calculus, which approximates discrete uncorrelated fluctuations as continuous white noise. Atmosphere and ocean processes are often represented by the Stratonovich calculus, in which rapidly fluctuating quantities with small but finite correlation times are parameterized as white noise. This paper makes use of the Itô interpretation, because this allows us to interpret the deterministic term $\mathbf{A}(\mathbf{x})$ as the effective drift and because it produces tractable equations that allow us to explore the role of stochastic processes in driving the ocean. For a detailed discussion of stochastic integration and the differences between Itô and Stratonovich SDEs see, for example, Horsthemke and Lefever (1984) or Gardiner (1985). In both calculi, the matrix $\mathbf{B}(\mathbf{x})$ describes the variability of the state vector $\mathbf{x}$ as a function of the state itself. For example, a state-dependent noise term is required to model the gustiness of synoptic sea surface winds (Sura, 2003).

The probability density function $p(\mathbf{x}, t)$ (PDF) of the Itô-SDE (1) is governed by the corresponding Fokker-Planck equation (e.g., Gardiner, 1985; Horsthemke and Lefever, 1984; Paul and Baschnagel, 1999):

$$\frac{\partial p(\mathbf{x}, t)}{\partial t} = -\sum_i \frac{\partial}{\partial x_i} A_i p(\mathbf{x}, t) + \frac{1}{2} \sum_{i,j} \frac{\partial^2}{\partial x_i \partial x_j} (\mathbf{B}\mathbf{B}^T)_{ij} p(\mathbf{x}, t). \tag{3}$$

The Fokker-Planck equation describes the conservation of the probability density $p(\mathbf{x}, t)$ of the system described by the SDE. The first term on the right describes the dynamics of the deterministic system and is called the deterministic drift. The second term causes the diffusion of the system.

Equations for the second moments of $\mathbf{x}$, representing variance or Reynolds stresses for example, can be obtained by multiplying the Fokker-Planck equation (3) by $x_p x_q$ and integrating over the domain of the system. That is,

$$\frac{\partial \langle x_p x_q \rangle}{\partial t} = \langle A_p x_q \rangle + \langle A_q x_p \rangle + \sum_i \langle B_{pi} B_{qi} \rangle. \tag{4}$$

This equation is known as the generalized fluctuation-dissipation relation (GFDR) of the system (see e.g., Penland, 1996). The GFDR relates the variance of the stochastic fluctuations to the magnitude of the dissipation.

The deterministic and stochastic parts of (3) can be determined directly from data by using their statistical definitions:

$$\mathbf{A}(\mathbf{x}) = \lim_{\Delta t \to 0} \frac{1}{\Delta t} \langle \mathbf{X}(t + \Delta t) - \mathbf{x} \rangle |_{\mathbf{X}(t) = \mathbf{x}} \tag{5}$$

$$\mathbf{B}(\mathbf{x})\mathbf{B}^T(\mathbf{x}) = \lim_{\Delta t \to 0} \frac{1}{\Delta t} \langle (\mathbf{X}(t + \Delta t) - \mathbf{x})(\mathbf{X}(t + \Delta t) - \mathbf{x})^T \rangle |_{\mathbf{X}(t) = \mathbf{x}} \tag{6}$$

where $\mathbf{X}(t + \Delta t)$ is a solution (a single stochastic realization) of the SDE (1) with the initial condition $\mathbf{X}(t) = \mathbf{x}$ at time t. The data define a state space representing every observed value of $\mathbf{x}$. Deterministic and stochastic parts of the underlying dynamics can be estimated at every point $\mathbf{x}$ at which there are sufficient observations. In order to obtain an estimate from discrete observations, the theoretical limit $\Delta t \to 0$ is replaced by a finite-difference approximation. Note that estimating the deterministic drift and stochastic diffusion parameters from discretely sampled data is fraught with the potential for error. See Sura (2003) or Sura and Barsugli (2002) for the error estimation in the case of a finite time increment Δt.

Analytical functions can be fitted to the empirical estimates of $\mathbf{A}(\mathbf{x})$ and $\mathbf{B}(\mathbf{x})\mathbf{B}^T(\mathbf{x})$ to derive model equations describing the system under consideration. In order to verify the results, the estimated functions $\mathbf{A}(\mathbf{x})$ and $\mathbf{B}(\mathbf{x})\mathbf{B}^T(\mathbf{x})$ can be inserted into the Fokker-Planck equation (3), and the resulting PDF can be compared with the PDF obtained directly from the data.

Note that $\mathbf{B}(\mathbf{x})\mathbf{B}^T(\mathbf{x})$ rather than $\mathbf{B}(\mathbf{x})$ is estimated from data. In general it is impossible to find a unique expression for $\mathbf{B}(\mathbf{x})$ in the multivariate case. However, in the univariate case $B(x) = \sqrt{B(x)^2}$. The sign of the square root is arbitrary because $B(x)$ is multiplied by Gaussian white noise with zero mean. Thus, in the univariate case even the SDE (1) can be used to test the estimates of $A(x)$ and $B(x)$ by simply comparing the properties (e.g., moments, spectra etc.) of the original time series with the properties of the time series obtained by integrating (1).

The technique described here has been successfully applied to a wide class of problems. For example, Friedrich and Peinke (1997a,b) and Renner *et al.* (2001) describe statistical properties of a turbulent cascade. Friedrich *et al.* (2000a) quantify deterministic and stochastic influences on the foreign exchange market. Geophysical examples are provided by Ditlevsen (1999), who fitted a Fokker-Planck equation to ice core data, and Egger

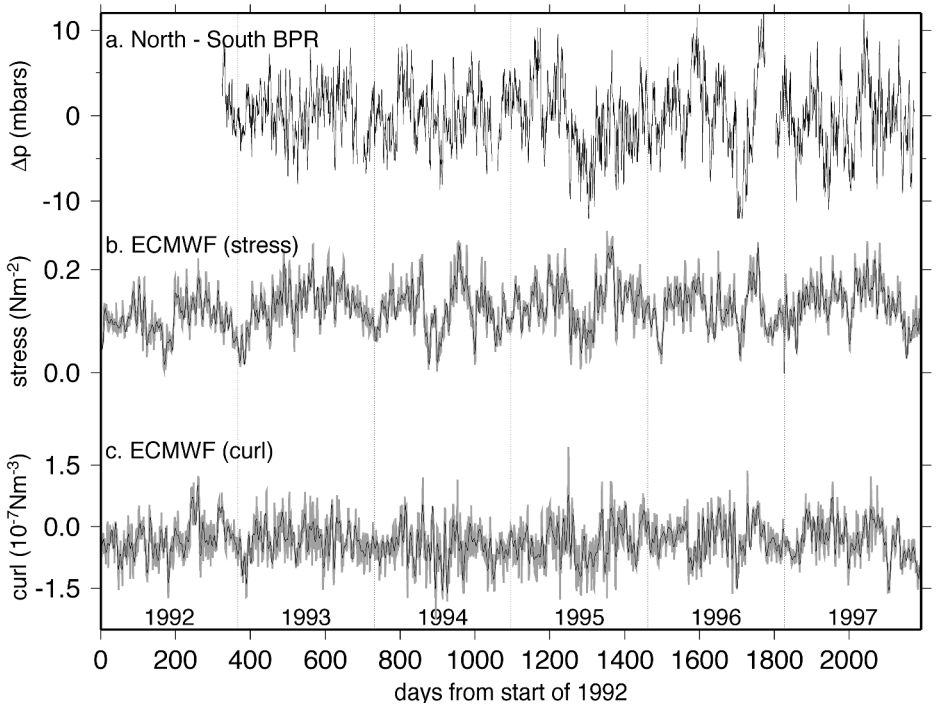

Figure 1. Time series of the data used in this study: (a) Bottom pressure difference across Drake Passage, (b) averaged wind stress, and (c) averaged wind stress curl. For the winds, original data are shaded, and data filtered to retain only time periods longer than 10 days are solid.

(2001), Egger and Jonsson (2002), and Sura (2003), who stochastically describe meteorological data sets.

3. Data

Here we examine the response of the ACC transport to wind stress forcing by analyzing bottom pressure and wind reanalysis products within a stochastic framework. The data used in this study have been used previously to study ACC transport variability in relation to wind forcing (e.g. Gille, 1999; Gille *et al.,* 2001). Bottom pressure gauges were deployed on either side of Drake Passage from November 1992 through November 1997 by Proudman Oceanographic Laboratory. As in previous studies, here we infer geostrophic transport fluctuations from the time-varying pressure difference across Drake Passage, shown in Figure 1. The original data were sampled at 15 min or hourly intervals, filtered to remove the semidiurnal/diurnal tidal signal, and subsampled at 12-hour intervals. Gaps in the pressure difference data are filled by linear interpolation.

Winds are represented by European Centre for Medium-Range Weather Forecasts (ECMWF) reanalysis for the 5-year period between 1992 and 1997. The wind stress and

the wind stress curl are averaged zonally over the full Southern Ocean and meridionally between 50S and 60S, corresponding to the approximate latitude band of the ACC at Drake Passage. Figure 1 shows the time series for wind stress and wind-stress curl. Note that the averaged zonal wind stress is very rarely negative. In the following all time series are normalized to have zero mean and unit standard deviation. For a more detailed description and a coherence analysis of the data see Gille *et al.* (2001).

4. Empirical stochastic models of the ACC

The mechanisms controlling ocean response to wind forcing depend on both the wind and the ocean transport. For this two component system, the governing SDE is

$$\begin{aligned} \frac{dx_1}{dt} &= A_1(x_1, x_2) + \sigma_1\eta_1 \\ \frac{dx_2}{dt} &= A_2(x_1, x_2) + \sigma_2\eta_2 \end{aligned} \tag{7}$$

where x_1 represents the wind stress in Section 4a, and wind stress curl in Section 4b, and x_2 is the pressure difference across Drake Passage. A number of studies have shown that atmospheric variability can be modeled by a stochastic process (e.g., Egger and Jonsson, 2002; Sura, 2003). The deterministic part represents the net slowly varying motion, which is excited by fast varying synoptic disturbances that are effectively stochastic. The same idea can be applied to the oceanic motion, where eddies, waves and other fast varying processes are parameterized by the noise component. This simple representation of the real world omits some important physical processes. Nevertheless, despite (or because of) their simplicity, empirical stochastic models have been proven to be useful diagnostic and forecasting tools (Ditlevsen, 1999; Egger, 2001; Egger and Jonsson, 2002; Sura, 2003; von Storch and Zwiers, 1999). Our findings show that the oceanic transport does not affect the atmospheric wind field, so that $A_1(x_1, x_2) = A_1(x_1)$. Note that (7) and all subsequent equations are dimensionless because the data are normalized.

In our analysis, we make two assumptions. First, the atmospheric wind field is expected to be unaffected by oceanic noise, and vice versa. Based on this assumption, the governing equations are simplified by assuming that the matrix $\mathbf{B}$ is diagonal with elements σ_1 and σ_2. As discussed later, this assumption can be tested a posteriori by using the GFDR (4). Second, in this section the noise term is not treated as a function of the state of the system. This means that the matrix $\mathbf{B}$ is assumed to be constant. The first assumption is physically reasonable, but the second assumption is an approximation that is not generally valid. As Sura (2003) has shown, a proper stochastic description of synoptic midlatitude sea surface winds requires a multiplicative noise component. The advantage of representing the wind stress as a red-noise process with constant $\mathbf{B}$ is that the resulting SDE (7) can then be handled analytically. The impact of a more realistic stochastic wind stress forcing on the wind driven ACC variability will be discussed in Section 5.

To evaluate A_1, A_2, σ_1, and σ_2 numerically, using the two-dimensional versions of Eqs. (5) and (6), the interval spanned by the data is divided into 24×24 equal bins. (Sensitivity experiments with different numbers of bins were performed as well, but the general results discussed below did not change.) Because in this section the stochastic terms are treated as constants, the results of Eq. (6) are averaged to obtain σ_1 and σ_2. Then, σ_1 and σ_2 are cross-checked by comparing the direct numerical estimates with the results obtained from the GFDR. The smallest possible discrete time step of half a day is used for Δt in the finite-difference approximation. Since the method assumes that the data are Markovian, we verify that the method yields stable and physically reasonable results for different discrete time steps Δt. A lack of convergence could indicate that the process had non-Markovian properties; however, in this study the results converge stably as Δt decreases, and the results are therefore consistent with the assumption that the data are Markovian. In particular, the results are approximately the same for time steps of $\Delta t = 12$, 24, and 36 h. That is, the error terms proportional to Δt (see Sura, 2003; Sura and Barsugli, 2002) are small and negligible for those time steps. The estimates diverge for time steps equal to or larger than 48 h.

In the following standard errors (standard deviation/$\sqrt{N}$) are used to quantify the uncertainties of the estimated parameters and related quantities.

a. Bottom pressure versus wind stress

The deterministic part of the wind stress time series, $A_1(x_1)$, is shown in Figure 2. The term $A_1(x_1)$ decreases with increasing values of x_1, meaning that it acts to damp the wind stress, and can be approximated by a linear function. This means that as a first approximation the wind stress can be represented as a univariate Ornstein-Uhlenbeck process. The decorrelation time scale is the inverse of the (dimensional) damping coefficient, which therefore is the typical damping time scale of the system under consideration. In these data the atmospheric decorrelation time scale appears to be about 10 days for the zonally and meridionally averaged wind stress. The local decorrelation time scale is much shorter, about 1 day (Sura, 2003).

The estimated function $A_2(x_1, x_2)$ is shown in Figure 3a, the related standard error is shown in Figure 3b. The uncertainties are relatively large: the standard error is about 0.05–0.1 for most of the points. Because of the large uncertainty, we performed tests in order to see whether the same results could be found in random, uncorrelated time series. Our tests showed that the qualitative structure of $A_2(x_1, x_2)$ (discussed below) could not be reproduced by such a random process. As a second test of the robustness of the results, we compared the original data with the time series obtained by integrating the SDE. This analysis concentrates on the qualitative aspects of the results which are robust and physically consistent. The deterministic part of the oceanic time series consists of a forcing and damping term. The forcing can be identified by the overall positive gradient of $A_2(x_1, x_2)$ in the direction of x_1, whereas the damping is due to the dominant negative gradient in the direction of x_2. The function $A_2(x_1, x_2)$ can be approximated by a planar fit. Assuming

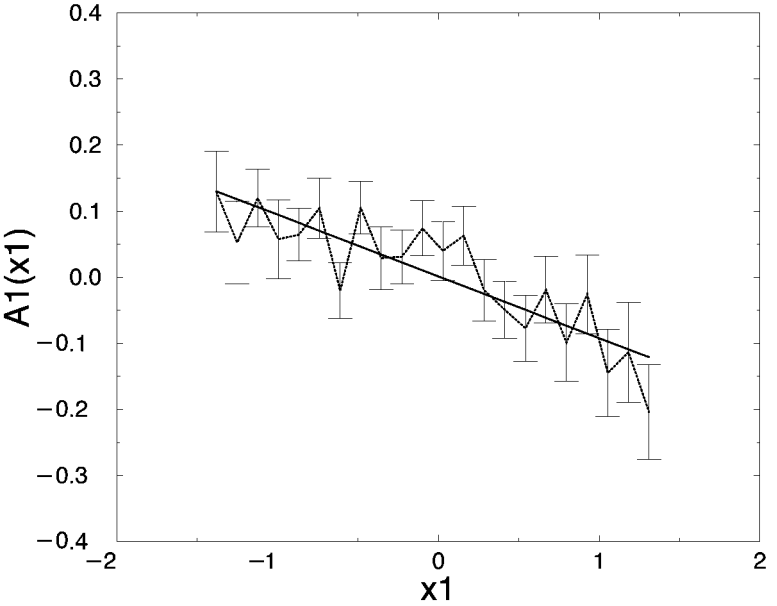

Figure 2. The estimated deterministic drift $A_1(x_1)$ for the wind stress x_1. The dashed line shows the actual estimated function. The solid line is a linear fit: $A_1(x_1) = -0.10(\pm 0.01)x_1$. The error bars indicate $\pm$ one standard error.

a linear fit to the entire deterministic drift (see Table 1) the corresponding two-dimensional SDE is

$$\begin{aligned} \frac{dx_1}{dt} &= -ax_1 + \sigma_1\eta_1 \\ \frac{dx_2}{dt} &= -bx_2 + cx_1 + \sigma_2\eta_2. \end{aligned} \tag{8}$$

See the Appendix for more details on multivariate Ornstein-Uhlenbeck processes such as this.

At this point the assumption that the matrix $\mathbf{B}$ is diagonal can be tested by a straightforward application of the GFDR (4). If the linear deterministic drift in (8) is written as a matrix $\mathbf{A}$ multiplied by the vector $\mathbf{x}$, the stationary GFDR becomes $\mathbf{BB}^T = -\mathbf{AC} - \mathbf{CA}^T$, where $\mathbf{C}$ denotes the covariance matrix. Thus, $\mathbf{BB}^T$ can be determined from the deterministic drift and the covariance matrix obtained from data. Inserting the drift and the covariance matrix into the GFDR reveals that the off-diagonal elements of $\mathbf{BB}^T$ are negligible relative to the diagonal elements: $BB^T_{1,2} = BB^T_{2,1} = 0.00 \pm 0.01$, $BB^T_{1,1} = 0.20 \pm 0.02$, $BB^T_{2,2} = 0.06 \pm 0.02$. The ratio of the off-diagonal elements to the smallest diagonal element is $BB^T_{1,2}/BB^T_{2,2} = 0.00 \pm 0.17$. Therefore, the noise terms are uncorrelated to a good approximation, and $\mathbf{B}$ can be treated as a diagonal matrix.

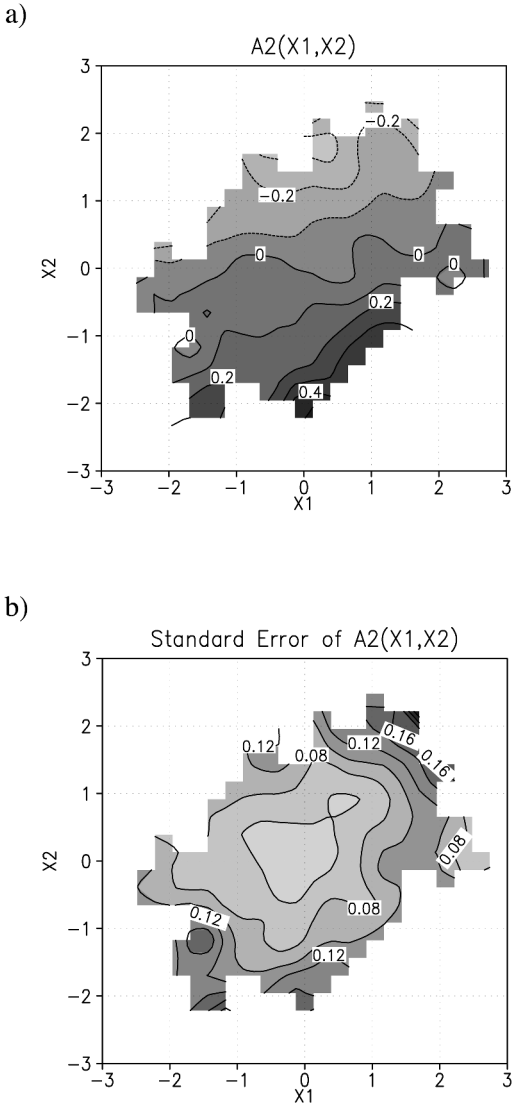

Figure 3. (a) The estimated deterministic drift $A_2(x_1, x_2)$ for the bottom pressure difference x_2. The contour and shading interval is 0.1. A planar fit yields: $A_2(x_1, x_2) = 0.04(\pm 0.01)x_1 - 0.04(\pm 0.01)x_2$. (b) The standard error of the estimated deterministic drift $A_2(x_1, x_2)$. The contour and shading interval is 0.02.

Since the noise matrix **B** is diagonal, the covariance matrix of (8) can be evaluated analytically to calculate the spectra and cross-spectra by Fourier transforming the appropriate elements of the covariance matrix: see (A.6), (A.7), and (A.8). Using the GFDR (or the

Table 1. Parameters (± one standard error) of the stochastic model (8): Wind stress and wind stress curl versus bottom pressure difference. Note that for the "curl versus bottom pressure" model σ_1^2 and σ_2^2 are not defined, because in that case the matrix **B** is nondiagonal.

Parameter	Stress versus bottom pressure	Curl versus bottom pressure
a	0.10 ± 0.01	0.24 ± 0.01
b	0.04 ± 0.01	0.04 ± 0.01
c	0.04 ± 0.01	0.03 ± 0.01
σ_1^2	0.18 ± 0.02	—
σ_2^2	0.05 ± 0.01	—

covariance matrix) and assuming stationary statistics, the first moments of the variables x_1 and x_2 can be obtained:

$$\langle x_1^2 \rangle = \frac{\sigma_1^2}{2a}$$

$$\langle x_2^2 \rangle = \frac{c}{b} \langle x_1 x_2 \rangle + \frac{\sigma_2^2}{2b} = \frac{c^2 \sigma_1^2}{2ab(a+b)} + \frac{\sigma_2^2}{2b} \tag{9}$$

$$\langle x_1 x_2 \rangle = \frac{c}{(a+b)} \langle x_1^2 \rangle = \frac{c\sigma_1^2}{2a(a+b)}.$$

The estimated parameters are summarized in Table 1. These parameters and the equation for $\langle x_2^2 \rangle$ together indicate that about 30(±10)% of ACC variability is driven by the wind stress, whereas about 70(±20)% is due to processes that are not included in our simple model, and are, therefore, parameterized as noise. Note that within our simple model the coupling of the wind stress and the ACC transport, that is the covariance $\langle x_1 x_2 \rangle$, depends linearly on the variance $\langle x_1^2 \rangle$ of the wind forcing.

The parameters derived in (8) can be used to estimate the spectral coherence of the wind with ACC transport and the phase difference between the two systems. Figure 4 shows the results of this estimation. The negative values of the phase ϕ indicate that the wind stress leads the oceanic transport. Figure 4 indicates that for time periods longer than about 100 days, wind stress and transport have constant and relatively high coherence. The coherence rapidly decreases for periods below 100 days. In the high coherence regime the oceanic transport lags the atmospheric forcing by about 60° for periods of 100 days; the phase lag becomes zero for very low frequencies (or long periods). Deterministic models suggest that at high frequencies wind should accelerate the ocean velocity, so that ACC transport lags wind by 90°. However, because of the low coherence at high frequencies, phase lags near 90° are not observed within the stochastic framework.

We test the estimates of $A_1(x_1)$, $A_2(x_1, x_2)$, σ_1, and σ_2 obtained by integrating (8) against the original bottom pressure difference time series. This is done by comparing the

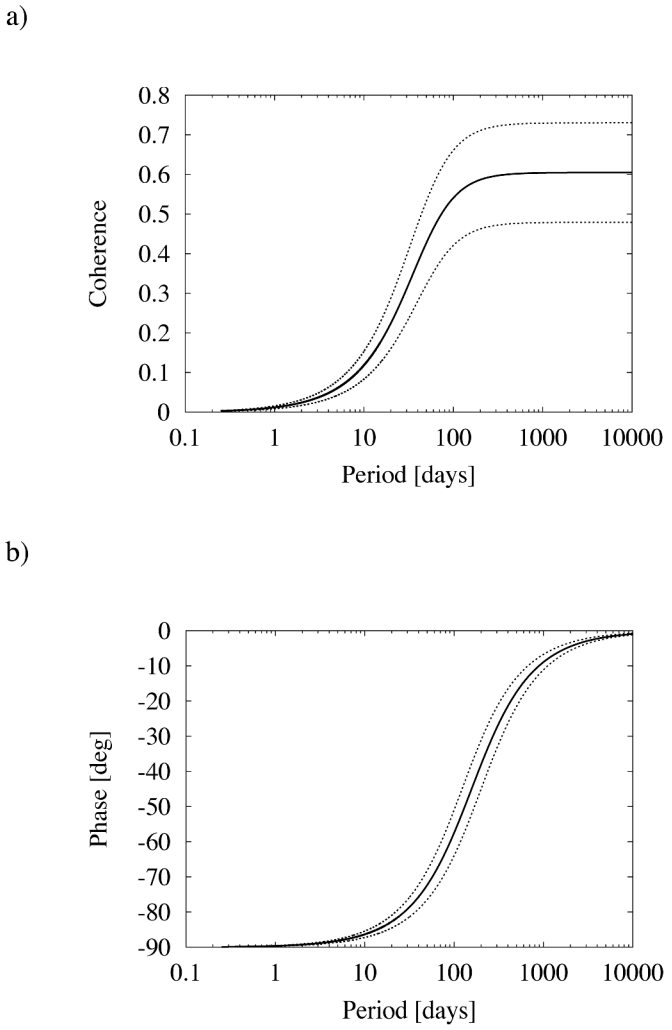

Figure 4. (a) Coherence and (b) phase spectra (solid lines) of the stochastic process (8) fitted to wind stress and bottom pressure difference. For clarity, the period is given in dimensional units, even if the data are nondimensional. The dotted lines indicate the error margins ($\pm$ one standard error).

spectra and histograms of the original data with the corresponding "artificial" data (see Fig. 5). SDE (8) is solved by the stochastic Euler scheme (see e.g., Kloeden and Platen, 1992).

Figure 5a shows the spectra of the original data and of the artificial data simulated by the stochastic model. Both indicate red noise behavior (with slopes $\propto \omega^{-2}$), as expected from the stochastic climate scenario proposed by Hasselmann (1976). A striking difference can be seen in the spectra at very high frequencies. The stochastic model does not reproduce the steep dip of the original data at frequencies of about 0.3 cycles per 0.5 days. The

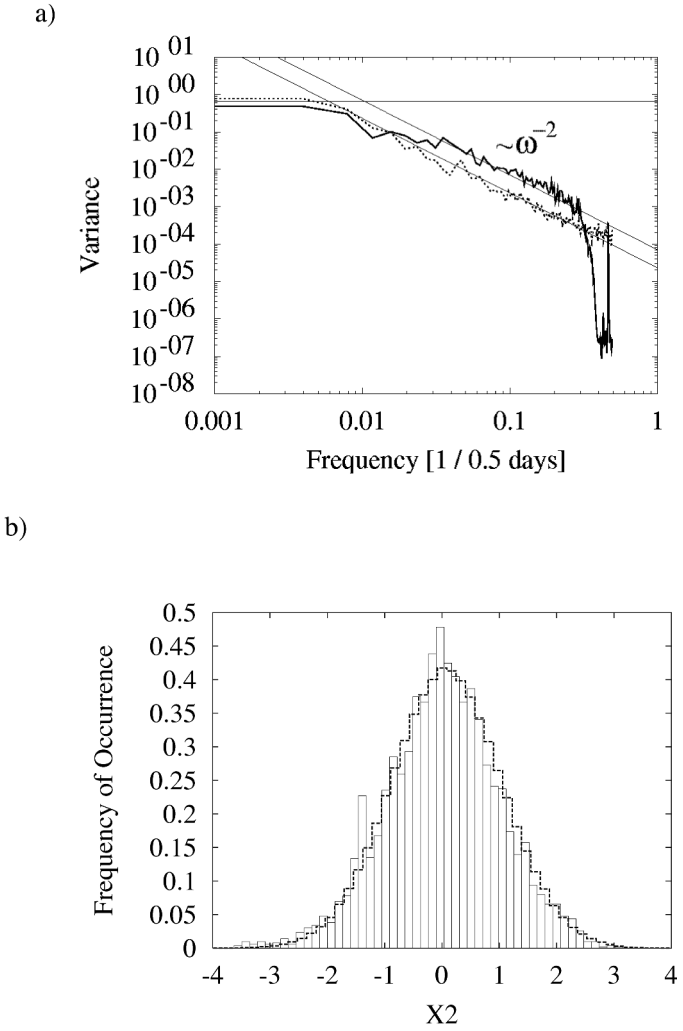

Figure 5. (a) Spectra and (b) histograms of the original ACC transport data from bottom pressure (solid lines) and the corresponding artificial data obtained by the SDE using the estimated parameters (dashed lines). The spectral slopes $\propto \omega^{-2}$ and $\propto \omega^{0}$ are indicated by the thin solid lines. For clarity, the frequency is given in dimensional units, even if the data are nondimensional.

low-pass filter used to remove tidal signals has removed high-frequency energy from the observations, but that effect is not reproduced by the stochastic model. It is known that Markov models are not capable of reproducing steep spectral dips at very high frequencies (DelSole, 2000). Because by construction both the original and the artificial data have the same overall variance, the spectra differ for frequencies below about 0.3 cycles per 0.5 days, even though the slopes are identical.

Figure 5b shows the histograms of the original data and of the linear stochastic model. Of course, the linear stochastic model produces a Gaussian distribution. Even the bottom pressure data are indistinguishable from a Gaussian distribution on the basis of the Kolmogorov-Smirnov test up to the 95% significance level. Nevertheless, more sophisticated methods like the Anderson-Darling or the Shapiro-Wilk test (NIST/SEMATECH, 2002) reveal that the bottom pressure data are actually non-Gaussian at the 99% significance level. The results of the different tests show that the data are weakly non-Gaussian, and that these subtle effects are not reproduced by the linear stochastic model.

To summarize, the linear stochastic model reproduces the general spectral characteristics of the original data. Furthermore, the stochastic method yields results that are qualitatively similar to those obtained by Gille *et al.* (2001) using coherence analysis. The linear stochastic model does not reproduce a constant phase lag of about 20° observed by Gille *et al.* (2001). This may occur because the constant phase lag observed in the data is a nonlinear effect that is neglected within the linear approximation of the deterministic term $A_2(x_1, x_2)$. Nevertheless, the linear stochastic model reproduces the observational result indicating that the coherence increases with increasing period.

b. Bottom pressure versus wind stress curl

In this section, we explore the relation of ACC transport variability to wind stress curl. In this case, the term $A_1(x_1)$ acts to dampen the wind stress curl nearly linearly (not shown), with a damping time scale of about 4–5 days. The estimated function $A_2(x_1, x_2)$ (not shown) is qualitatively similar to the results based on wind stress shown in Figure 3: the deterministic part of the oceanic time series consists of a forcing and damping term, and the function $A_2(x_1, x_2)$ can again be approximated by a planar fit. See Table 1 for the estimated deterministic parameters. Again, the assumption that the matrix $\mathbf{B}$ is diagonal can now be tested by using the stationary GFDR $\mathbf{BB}^T = -\mathbf{AC} - \mathbf{CA}^T$. However, inserting the drift and the covariance matrix into the GFDR now reveals that the off-diagonal elements of $\mathbf{BB}^T$ are not negligible relative to the diagonal elements: $BB^T_{1,2} = BB^T_{2,1} = 0.03 \pm 0.01$, $BB^T_{1,1} = 0.43 \pm 0.03$, $BB^T_{2,2} = 0.04 \pm 0.03$. The ratio of the off-diagonal elements to the smallest diagonal element is $BB^T_{1,2}/BB^T_{2,2} = 0.75 \pm 0.62$. In this case the matrix $\mathbf{B}$ is not diagonal and the assumption of uncorrelated noises in each dimension is not valid. Thus, the correlation between curl and pressure is partly due to the covariance structure of the noise terms. Because this spurious coupling due to the noise involves another parameterized (and therefore unknown) mechanism, transport fluctuations appear more likely to be driven by wind stress than wind stress curl.

c. The stochastic Wearn-Baker model

As a first approximation the response of the ACC to wind stress forcing can be understood in terms of the stochastic version of the simple model introduced by Wearn and Baker (1980). In their model the time evolution of the transport $U(t)$ is simply due to the wind stress $\tau_x(t)$ and a linear drag term scaled by b:

$$\frac{\partial U}{\partial t} = -bU + \tau_x(t). \tag{10}$$

Wearn and Baker (1980) derived an analytic solution for a deterministic sinusoidal forcing $\tau_x(t) = \tau_0 \exp(i\omega t)$. The solution of the "deterministic Wearn-Baker model" is

$$U(t) = \frac{\tau_0}{\sqrt{b^2 + \omega^2}} \exp(i\omega t - \phi), \tag{11}$$

where $\phi = \arctan(-\omega/b)$. Therefore, in the sinusoidally forced deterministic case the variance of the transport becomes

$$\langle U^2(t) \rangle = \frac{\pi \tau_0^2}{(b^2 + \omega^2)}. \tag{12}$$

The previous results showed that the ocean transport appears to be driven by a stochastic red noise wind stress forcing (neglecting the multiplicative character of the wind stress forcing to be discussed in Section 5). The governing SDE for the wind stress is

$$\frac{d\tau_x}{dt} = -a\tau_x + \eta \tag{13}$$

with the Gaussian white noise η. The solution for the wind stress is

$$\tau_x(t) = \exp(-at) \int_0^t \exp(as) dW(s). \tag{14}$$

where dW is the incremental change of the Wiener process W. Using this red noise process to force the model (10) the variance of the transport in the "stochastic Wearn-Baker model" becomes

$$\langle U^2(t) \rangle = \frac{\langle \tau_x^2 \rangle}{(b^2 + ab)}. \tag{15}$$

Thus the variance in (15) resembles the variance from the Wearn-Baker model, (12), with the deterministic frequency term, ω^2, replaced by the product of the inverse atmospheric and oceanic decorrelation time scales ab.

5. The role of multiplicative noise

a. Multiplicative noise in stochastic forcing

This section examines how multiplicative wind forcing alters the linear stochastic models derived in Section 4. The one-dimensional SDE to describe the wind stress data is now written as

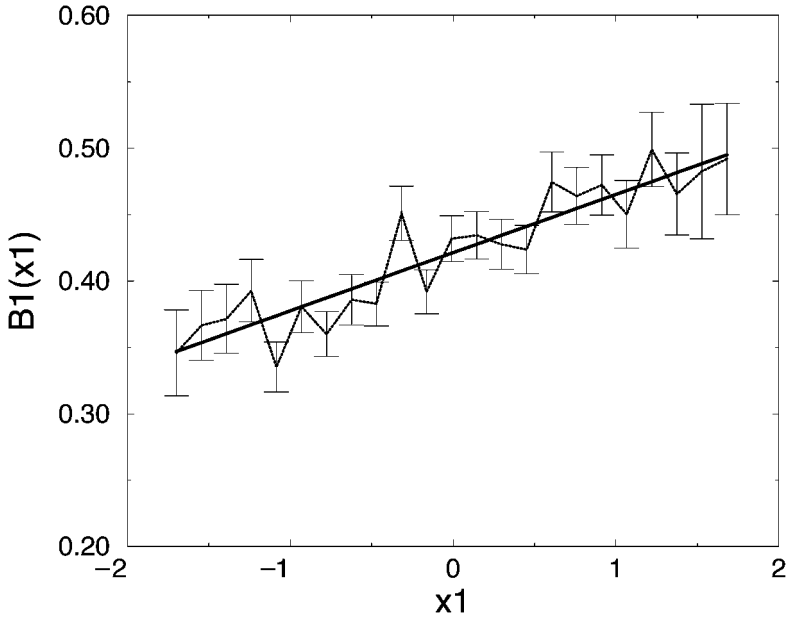

Figure 6. The estimated noise $B_1(x_1)$ for the wind stress x_1. The dashed line shows the actual estimated function. The solid line is a linear fit: $B_1(x_1) = 0.044(\pm 0.005)x_1 + 0.42(\pm 0.005)$. The error bars indicate $\pm$ one standard error.

$$\frac{dx_1}{dt} = A_1(x_1) + B_1(x_1)\eta_1 \tag{16}$$

where x_1 is the wind stress, $A(x_1)$ is the deterministic, and $B_1(x_1)\eta_1$ the stochastic part. As shown in Section 4a and in Figure 2, the deterministic term $A_1(x_1)$ acts to dampen the wind stress and can be approximated by a linear function. Note that the multiplicative noise $B_1(x_1)$ can be calculated directly from (6) at every point x_1 whose neighborhood is visited often enough by the data trajectory. In the previous section the average was used to neglect the state dependence of the noise. In this section, the function $B_1(x_1)$ is no longer held constant, but depends on the state of the system, as shown in Figure 6. The amplitude of the white noise forcing increases approximately linearly with increasing wind stress values. Therefore, the behavior of the multiplicative noise in the averaged wind stress data is qualitatively consistent with the results obtained by Sura (2003), who used local winds to show that the variability of midlatitude winds increases with increasing wind speed. His results suggested that a more complete stochastic description of the wind stress data would require a state dependent white noise forcing term. As a result of this state-dependent forcing, an Ornstein-Uhlenbeck process is not sufficient to describe the wind stress data within a stochastic framework.

b. Stochastic Wearn-Baker driven by a multiplicative wind stress forcing

Most stochastically forced ocean models implement the atmospheric stochastic forcing as *Gaussian* white or red noise. In the red noise case, the atmosphere is often modeled by a univariate Ornstein-Uhlenbeck process such as (13). There, the strength of the atmospheric noise is held constant and does not depend on the state of the system. However, as shown in the previous section, a more accurate stochastic description of the wind stress data requires a state dependent white noise forcing term. It is well known that a multiplicative stochastic process generates a power-law distribution in contrast with the Gaussian distribution of an Ornstein-Uhlenbeck process (e.g., Schenzle and Brand, 1979; Succi and Iacono, 1986; Sakaguchi, 2001). In this section the stochastic Wearn-Baker model serves as a toy-model to illustrate the effect of a more realistic *non-Gaussian* wind forcing on the variability of the oceanic circulation. We will consider the following stochastic model:

$$\frac{d\tau}{dt} = -a\tau + \sqrt{2M}\,|\tau|\eta_M + \sqrt{2D}\,\eta_D$$
$$\frac{dU}{dt} = -bU + \tau \tag{17}$$

with Gaussian white noise satisfying

$$\langle \eta_M(t)\eta_M(t')\rangle = \delta(t - t'), \qquad \langle \eta_D(t)\eta_D(t')\rangle = \delta(t - t'). \tag{18}$$

M and D are constants governing the strength of the additive and multiplicative noise terms. The first equation models the wind stress τ by a simple linear damping term, and a combination of a state dependent and constant noise terms. The ocean transport U is driven solely by the stochastic wind stress and retarded by a linear damping term. This simplistic representation of the ocean parameterizes the fact that parts of oceanic variability are driven by the wind, whereas other effects tend to dampen the oceanic motions. Thus, this simple model can serve as a toy-model to illustrate the basic effect of a non-Gaussian wind forcing on the variability of the oceanic circulation.

The stationary PDF of the wind stress τ has the form (Sakaguchi, 2001):

$$p(\tau) = \Theta(D + M\tau^2)^{-\Pi} \tag{19}$$

with $\Pi = (a + 2M)/2M$. The normalization constant Θ is given by:

$$\Theta = \frac{M^{1/2}D^{\Pi-1/2}}{\beta(1/2,\ \Pi - 1/2)} = \frac{M^{1/2}D^{\Pi-1/2}\Gamma(\Pi)}{\Gamma(1/2)\Gamma(\Pi - 1/2)} \tag{20}$$

where $\beta(x, y)$ is the beta function, and $\Gamma(x)$ is the gamma function: $\beta(x, y) = \Gamma(x)\Gamma(y)/\Gamma(x + y)$. The variance of the wind stress τ can be calculated as

$$\int_{-\infty}^{\infty} \tau^2 p\, d\tau = \langle \tau^2 \rangle = \frac{D}{a - M}. \tag{21}$$

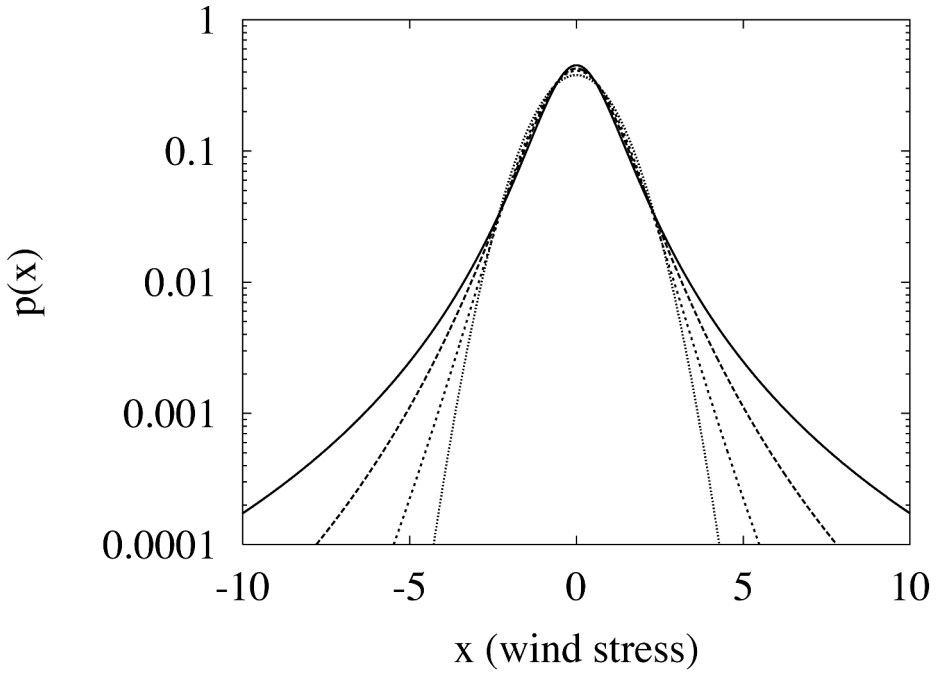

Figure 7. Stationary wind stress probability distributions $p(\tau)$ given by Eqs. (19) and (20) for $a = 1$, $D = 1$, and different strengths of the multiplicative noise: $M = 0.5$ (solid line), $M = 0.25$ (long dashed line), $M = 0.1$ (short dashed line), and $M \to 0$ (dotted line). For $M \to 0$ the distribution becomes Gaussian with the variance D/a.

Figure 7 shows distributions $p(\tau)$ as defined by Eqs. (19) and (20) for $a = 1$, $D = 1$, with different strengths of the multiplicative noise M. For $M \to 0$, the distribution becomes Gaussian with the variance D/a. The multiplicative noise causes the tails of the distribution to be heavier than they would be in the corresponding Gaussian distribution.

For the limits of very large and small b the probability distribution of U can be determined analytically. For large b the time derivative of U can be neglected:

$$U = \frac{\tau}{b} \tag{22}$$

Therefore,

$$\frac{dU}{dt} = \frac{1}{b}\frac{d\tau}{dt} = -aU + \sqrt{2M}\,|U|\eta_M + \sqrt{2D}\,\frac{\eta_D}{b}. \tag{23}$$

Thus, in (19) and (20) we substitute D/b^2 in place of D to obtain the distribution of U:

$$p(U) = \Upsilon\left(\frac{D}{b^2} + MU^2\right)^{-\Pi} \tag{24}$$

with the normalization constant Υ given by

$$\Upsilon = \frac{M^{1/2}(D/b^2)^{\Pi-1/2}}{\beta(1/2,\ \Pi - 1/2)}. \tag{25}$$

Thus, when friction b is large, ocean transport is expected to have a power-law distribution.

For small b, $dU/dt = \tau$ so $U = \Sigma_j \tau_j \Delta t$, and the central limit theorem applies. That means, the distribution $p(U)$ becomes Gaussian with the variance $\langle U^2 \rangle$, which is determined by the stationary version of the GFDR (4):

$$\langle U^2 \rangle = \frac{\langle \tau^2 \rangle}{b(a + b)} = \frac{D}{(a - M)b(a + b)}. \tag{26}$$

For intermediate b the distribution $p(U)$ will be somewhere in between the Gaussian and the power-law. More precisely, the damping b determines whether the PDF of the wind-driven oceanic flow is Gaussian (small damping) or resembles the distribution of the atmospheric forcing (large damping). This crude model of the wind-driven ocean circulation has interesting implications. Wind PDFs have been observed to be non-Gaussian almost everywhere. In contrast, ocean velocity PDFs are Gaussian throughout most of the ocean, except in a few specific regions, such as the Gulf Stream, which are usually associated with high eddy kinetic energy (Llewellyn Smith and Gille, 1998; Gille and Llewellyn Smith, 2000; Bracco *et al.,* 2000). If the effective dissipation b varies regionally depending on ocean eddy kinetic energy, then this model suggests that we should expect velocity PDFs to have different shapes in different locations.

6. Summary and discussion

An empirical stochastic model has been derived from wind stress and bottom pressure gauge data in order to examine the response of the Antarctic Circumpolar Current (ACC) transport to wind stress forcing. A general method is used to estimate the drift and diffusion coefficients of a continuous stationary Markovian system. As a first approximation, the response of the ACC to wind stress forcing can be described by a multivariate Ornstein-Uhlenbeck process: Gaussian red noise wind stress drives the evolution of the ACC transport that is damped by a linear drag term. The spectrum of the ACC transport fluctuations is red, as expected from the stochastic climate scenario proposed by Hasselmann (1976). The empirical model shows nearly the same behavior as revealed by coherence analysis of the same data set (Gille *et al.,* 2001). The linear stochastic model does not reproduce a constant phase lag of about 20° between wind stress and ACC transport as observed by Gille *et al.* (2001), but rather shows the classical frequency dependent phase (Wearn and Baker, 1980). The constant phase lag observed in the data is believed to be due to nonlinear effects that are not captured by the linear approximation. Despite this deficiency, the stochastic model can serve as a null hypothesis for studies of wind-driven ACC variability. That is, the stochastic Wearn-Baker model is actually the simplest null hypothesis that describes wind-driven ACC variability.

In light of Hasselmann's theory this is actually not a very surprising result, though it reinforces the importance of *stochastic climate models.* Much more important is the fact that stochastic descriptions of Southern Ocean wind stress are improved by using a multiplicative noise component. The variability of the wind stress increases with increasing wind stress values. This behavior has been discussed in more detail by Sura (2003). Most importantly, a multiplicative stochastic process generates a power-law distribution rather than a Gaussian distribution.

Using a simple linear stochastic model, it is shown that non-Gaussian forcing may have a significant impact on the velocity (or transport) PDFs of the wind driven ocean circulation. If the oceanic damping is small, the ocean has a very long memory, and oceanic velocities will represent a summation of many independent wind forcings. Then, as a result of the central limit theorem, the ocean velocities should have a Gaussian distribution, provided that the wind forcing PDF has finite variance. On the other hand, if the oceanic damping is large, the ocean has little memory, and ocean velocities will reflect wind velocities. In this case the wind driven velocities will have distributions like the wind forcing distributions. The real ocean must lie somewhere in between these extremes, sometimes showing Gaussian PDFs and sometimes PDFs that resemble those of the wind forcing. Note that in the real ocean velocity PDFs can also be non-Gaussian due to the nonlinear behavior of the ocean itself. Nevertheless, the implications of these results are clear: in order to interpret observed oceanic velocity PDFs in a physical meaningful sense, the impact of a non-Gaussian wind forcing on the ocean circulation will need to be explored in the future using more complicated models.

Acknowledgments. We thank the two anonymous reviewers for their valuable comments that led to improvements if the original manuscript. Bottom pressure data for this study are archived by the Proudman Oceanographic Laboratory at www.pol.ac.uk/psmslh/gloup/gloup.html. This work was funded through the NASA Ocean Vector Wind Science Team, JPL Contract number 1222984, and finished while P.S. was at the NOAA-CIRES Climate Diagnostics Center, funded by the Office of Naval Research, Grant N00014-99-1-0021.

APPENDIX

Multivariate Ornstein-Uhlenbeck process

In this Appendix the properties of the multivariate Ornstein-Uhlenbeck process are discussed briefly. For a more comprehensive discussion see e.g. Gardiner (1985), Horsthemke and Lefever (1984), or Kloeden and Platen (1992).

The multivariate Ornstein-Uhlenbeck process is defined by the Itô SDE

$$\frac{d\mathbf{x}}{dt} = \mathbf{A}\mathbf{x} + \mathbf{B}\boldsymbol{\eta}, \tag{A.1}$$

where $\mathbf{A}$ and $\mathbf{B}$ are constant $n \times n$ matrices. The stochastic components η_i are assumed to be independent Gaussian white noise processes:

$$\langle \eta_i(t) \rangle = 0, \qquad \langle \eta_i(t) \eta_i(t') \rangle = \delta(t - t') \tag{A.2}$$

where $\langle \cdot \rangle$ denotes the averaging operator. Eq. (A.1) can be rewritten in terms of a n-dimensional Wiener process $\mathbf{W}$:

$$d\mathbf{x} = \mathbf{A}\mathbf{x}dt + \mathbf{B}d\mathbf{W}. \tag{A.3}$$

The generalized derivative of a Wiener process is Gaussian white noise $\boldsymbol{\eta}$. Common examples of Wiener processes are Brownian motion or the continuous random walk. The solution of this SDE is given by (see e.g., Gardiner, 1985; Horsthemke and Lefever, 1984; Kloeden and Platen, 1992)

$$\mathbf{x}(t) = \exp(\mathbf{A}t)\mathbf{x}(0) + \int_0^t \exp[\mathbf{A}(t - t')]\mathbf{B}d\mathbf{W}(t'). \tag{A.4}$$

The solution requires the explicit knowledge of the matrix exponential function $\exp(\mathbf{A}t)$. The corresponding covariance matrix is

$$\begin{aligned} \langle \mathbf{x}(t)\mathbf{x}^T(s) \rangle = {} & \exp(\mathbf{A}t) \langle \mathbf{x}(0)\mathbf{x}^T(0) \rangle \exp(\mathbf{A}s) \\ & + \int_0^{\min(t,s)} \exp[\mathbf{A}(t - t')]\mathbf{B}\mathbf{B}^T \exp[\mathbf{A}^T(s - t')]dt'. \end{aligned} \tag{A.5}$$

The integral can be explicitly evaluated in certain special cases, as long as the matrix exponential function is known (see e.g. Braun (1993) for techniques to determine explicit expressions for matrix exponential functions). The spectra and cross-spectra can be evaluated by Fourier transforming the appropriate elements of the covariance matrix.

Using the stochastic process described by (9), the elements of the covariance matrix become:

$$\langle x_1(t)x_1(s) \rangle = \frac{\sigma_1^2}{2a} \exp(-a|t - s|) \tag{A.6}$$

$$\langle x_1(t)x_2(s) \rangle = \frac{\sigma_1^2 c}{2a(b - a)} \exp(-a|t - s|) - \frac{\sigma_1^2 c}{(b^2 - a^2)} \exp(-at - bs + (a + b) \min(t, s)) \tag{A.7}$$

$$\begin{aligned} \langle x_2(t)x_2(s) \rangle = {} & \frac{\sigma_1^2 c^2}{2a(b - a)^2} \exp(-a|t - s|) - \frac{\sigma_1^2 c^2}{(a + b)(b - a)^2} \exp(-at - bs + (a + b) \min(t, s)) \\ & - \frac{\sigma_1^2 c^2}{(a + b)(b - a)^2} \exp(-bt - as + (a+b) \min(t, s)) \\ & + \frac{\sigma_1^2 c^2}{2b(b - a)^2} \exp(-b|t - s|) + \frac{\sigma_2^2}{2b} \exp(-b|t - s|). \end{aligned} \tag{A8}$$

Note that the covariance matrix is of course symmetric: $\langle x_1(t)x_2(s) \rangle = \langle x_2(t)x_1(s) \rangle$.

REFERENCES

Berloff, P. S. and J. C. McWilliams. 2002. Material transport in oceanic gyres. Part II: Hierarchy of stochastic models. J. Phys. Oceanogr., *31,* 797–830.

Bracco, A., J. H. LaCasce and A. Provenzale. 2000. Velocity probability density functions for oceanic floats. J. Phys. Oceanogr., *30,* 461–474.

Braun, M. 1993. Differential Equations and Their Applications: An Introduction to Applied Mathematics, Springer-Verlag, 578 pp.

DelSole, T. 2000. A fundamental limitation of Markov models. J. Atmos. Sci., *57,* 2158–2168.

Ditlevsen, P. D. 1999. Observation of α-stable noise induced millenial climate changes from an ice-core record. Geophys. Res. Lett., *26,* 1441–1444.

Egger, J. 2001. Master equations for climatic parameter sets. Climate Dynamics, *18,* 169–177.

Egger, J. and T. Jonsson. 2002. Dynamic models for Icelandic meteorological data sets. Tellus A, *54,* 1–13.

Friedrich, R. and J. Peinke. 1997a. Description of a turbulent cascade by a Fokker-Planck equation. Phys. Rev. Lett., *78,* 863–866.

—— 1997b. Statistical properties of a turbulent cascade. Physica D, *102,* 147–155.

Friedrich, R., J. Peinke and C. Renner. 2000a. How to quantify deterministic and random influences on the statistics of the foreign exchange market. Phys. Rev. Lett., *84,* 5224–5227.

Friedrich, R., S. Siegert, J. Peinke, S. Lück, M. Siefert, M. Lindemann, J. Raethjen, G. Deusch and G. Pfister. 2000b. Extracting model equations from experimental data. Phys. Lett. A, *271,* 217–222.

Gardiner, C. W. 1985. Handbook of Stochastic Methods for Physics, Chemistry and the Natural Science, Second Edition, Springer-Verlag, 442 pp.

Gille, S. T. 1999. Evaluating Southern Ocean response to wind forcing. Phys. Chem. Earth, *24,* 423–428.

Gille, S. T. and S. G. Llewellyn Smith. 2000. Velocity probability density functions from altimetry. J. Phys. Oceanogr., *30,* 125–136.

Gille, S. T., D. P. Stevens, R. T. Tokmakian and K. J. Heywood. 2001. Antarctic Circumpolar Current response to zonally averaged winds. J. Geophys. Res., *106,* 2743–2759.

Gradišek, J., S. Siegert, R. Friedrich and I. Grabec. 2000. Analysis of time series from stochastic processes. Phys. Rev. E, *62,* 3146–3155.

Hasselmann, K. 1976. Stochastic climate models. Part I. Theory. Tellus, *28,* 473–484.

Horsthemke, W. and R. Lefever. 1984. Noise-Induced Transitions: Theory and Applications in Physics, Chemistry, and Biology, Springer-Verlag, 318 pp.

Hughes, C. W., M. P. Meredith and K. J. Heywood. 2000. Wind-driven transport fluctuations through Drake Passage: A southern mode. J. Phys. Oceanogr., *29,* 1971–1991.

Imkeller, P. and J.-S. von Storch, eds. 2001. Stochastic Climate Models, *in* Progress in Probability, *49,* Birkhäuser Verlag, 398 pp.

Kloeden, P. and E. Platen. 1992. Numerical Solution of Stochastic Differential Equations, Springer-Verlag, 632 pp.

Llewellyn-Smith, S. G. and S. T. Gille. 1998. Probability density functions of large-turbulence in the ocean. Phys. Rev. Lett., *81,* 5249–5252.

Munk, W. and E. Palmén. 1951. Note on the dynamics of the Antarctic Circumpolar Current. Tellus, *3,* 53–55.

NIST/SEMATECH. 2002. e-Handbook of Statistical Methods, http://www.itl.nist.gov/div898/handbook/.

Paul, W. and J. Baschnagel. 1999. Stochastic Processes: From Physics to Finance, Springer-Verlag, 231 pp.

Penland, C. 1996. A stochastic model of Indio Pacific sea surface temperature anomalies. Phys. D, *98,* 543–558.

Renner, C., J. Peinke and R. Friedrich. 2001. Experimental indications of Markov properties of small-scale turbulence. J. Fluid Mech., *433,* 383–409.

Rintoul, S., C. Hughes and D. Olbers. 2001. The Antarctic Circumpolar Current System, *in* Ocean Circulation and Climate, G. Siedler, J. Church, and J. Gould, eds., Academic Press, 271–302.

Sakaguchi, H. 2001. Fluctuation dissipation relation for a Langevin model with multiplicative noise. J. Phys. Soc. Jpn., *70,* 3247–3250.

Schenzle, A. and H. Brand. 1979. Multiplicative stochastic processes in statistical physics. Phys. Rev. A, *20,* 1628–1647.

Siegert, S., R. Friedrich and J. Peinke. 1998. Analysis of data sets of stochastic systems, Phys. Lett. A, *243,* 275–280.

Stommel, H. 1957. A survey of ocean current theory. Deep-Sea Res., *4,* 149–184.

Succi, S. and R. Iacono. 1986. Similarity solutions of the one-dimensional Fokker-Planck equation. Phys. Rev. A, *33,* 4419–4422.

Sura, P. 2003. Stochastic analysis of Southern and Pacific Ocean sea surface winds. J. Atmos. Sci., *60,* 654–666.

Sura, P. and J. J. Barsugli. 2002. A note on estimating drift and diffusion parameters from timeseries. Phys. Lett. A, *305,* 304–311.

von Storch, H. and F. W. Zwiers. 1999. Statistical Analysis in Climate Research, Cambridge University Press, 484 pp.

Wearn, R. B. and D. J. Baker. 1980. Bottom pressure measurements across the Antarctic Circumpolar Current and their relation to the wind. Deep-Sea Res., Part A, *27,* 875–888.

Weisse, R., U. Mikolajewicz, A. Sterl and S. S. Drijfhout. 1999. Stochastically forced variability in the Antarctic Circumpolar Current. J. Geophys. Res., *104,* 11049–11064.

Received: *13 August, 2002;* revised: *23 April, 2003.*